Atmos. Chem. Phys., 13, 6473–6491, 2013
www.atmos-chem-phys.net/13/6473/2013/
doi:10.5194/acp-13-6473-2013

Atmospheric Chemistry and Physics Open Access

Radical mechanisms of methyl vinyl ketone oligomerization through aqueous phase OH-oxidation: on the paradoxical role of dissolved molecular oxygen

P. Renard[1], F. Siekmann[1], A. Gandolfo[1], J. Socorro[1], G. Salque[3], S. Ravier[1], E. Quivet[1], J.-L. Clément[2], M. Traikia[5], A.-M. Delort[5,6], D. Voisin[3], V. Vuitton[4], R. Thissen[4], and A. Monod[1]

[1]Aix-Marseille Université, CNRS, LCE FRE3416, 13331, Marseille, France
[2]Aix Marseille Université, CNRS, ICR UMR7273, 13397, Marseille, France
[3]Université Joseph Fourier, Grenoble 1/CNRS-INSU, Laboratoire de Glaciologie et Géophysique de l'Environnement, 54 rue Molière, 38402 Saint-Martin-d'Hères, France
[4]Institut de Planétologie et d'Astrophysique de Grenoble (IPAG) UMR5274, UJF-Grenoble1/CNRS-INSU, Grenoble, 38041, France
[5]Clermont Université, Université Blaise Pascal, Institut de Chimie de Clermont-Ferrand, BP 10448, 63000 Clermont-Ferrand, France
[6]CNRS, UMR6296, ICCF, BP 80026, 63171 Aubière, France

Correspondence to: P. Renard (renard.pascal@yahoo.fr)

Received: 17 December 2012 – Published in Atmos. Chem. Phys. Discuss.: 28 January 2013
Revised: 3 June 2013 – Accepted: 4 June 2013 – Published: 8 July 2013

Abstract. It is now accepted that one of the important pathways of secondary organic aerosol (SOA) formation occurs through aqueous phase chemistry in the atmosphere. However, the chemical mechanisms leading to macromolecules are still not well understood. It was recently shown that oligomer production by OH radical oxidation in the aerosol aqueous phase from α-dicarbonyl precursors, such as methylglyoxal and glyoxal, is irreversible and fast.

Methyl vinyl ketone (MVK) was chosen in the present study as it is an α,β-unsaturated carbonyl that can undergo radical oligomerization in the aerosol aqueous phase. We present here experiments on the aqueous phase OH-oxidation of MVK, performed under various conditions. Using NMR and UV absorption spectroscopy, high and ultra-high resolution mass spectrometry, we show that the fast formation of oligomers up to 1800 Da is due to radical oligomerization of MVK, and 13 series of oligomers (out of a total of 26 series) are identified. The influence of atmospherically relevant parameters such as temperature, initial concentrations of MVK and dissolved oxygen are presented and discussed. In agreement with the experimental observations, we propose a chemical mechanism of OH-oxidation of MVK in the aqueous phase that proceeds via radical oligomerization of MVK on the olefin part of the molecule. This mechanism highlights in our experiments the paradoxical role of dissolved O_2: while it inhibits oligomerization reactions, it contributes to produce oligomerization initiator radicals, which rapidly consume O_2, thus leading to the dominance of oligomerization reactions after several minutes of reaction. These processes, together with the large range of initial concentrations investigated show the fundamental role that radical oligomerization processes likely play in polluted fogs and atmospheric aerosol.

1 Introduction

Although secondary organic aerosol (SOA) represents a substantial part of organic aerosol, which affects air quality, climate and human health, the understanding of its formation pathways and its properties is still limited due to the complexity of the physicochemical processes involved. It is now accepted that one of the important pathways of SOA formation occurs through aqueous phase chemistry (Hallquist et

al., 2009; Carlton et al., 2009; Ervens et al., 2011). In particular, a number of studies have observed the formation of large molecular weight compounds in atmospheric aerosols (see for example Claeys et al., 2004, 2010; Baduel et al., 2010; Liao and Seinfeld, 2005; Nozière et al., 2006) and in cloud/fog droplets (Herckes et al., 2002, 2007).

Recent studies have shown that (aerosol) aqueous phase chemistry of glyoxal (Volkamer et al., 2007, 2009; Ervens and Volkamer, 2010; Lim et al., 2010), methylglyoxal (Tan et al., 2012), pyruvic acid (Guzmàn et al., 2006; Tan et al., 2012) glycolaldehyde (Ortiz-Montalvo et al., 2012), methacrolein and methyl vinyl ketone (El Haddad et al., 2009; Liu et al., 2012) can produce significant amounts of SOA. In particular, Volkamer et al. (2007, 2009) and Ervens and Volkamer (2010) have shown that SOA production can occur via cloud and aerosol aqueous phase processes of glyoxal in deliquesced particles named wet aerosol, where ambient relative humidity (RH) ranges from 50 to 80 %. These findings give an extremely large set of conditions where organic aqueous phase processes can occur, i.e., from rain drop, cloud and fog droplet to wet aerosol, for which atmospheric lifetimes (< 1 min – days), liquid water content (LWC $\sim 10^8$–$1\,\mu g\,m^{-3}$), surface area of a particle, drop or droplet ($A = \pi D^2 \sim 10^{-2}$–$10^{-10}\,cm^2$), particle number concentration ($\sim 10^{-4}$–$10^4\,cm^{-3}$) and individual organic and inorganic chemical concentrations ($\sim 10^{-2}$–$10^6\,\mu M$) vary over orders of magnitude (Ervens and Volkamer, 2010). In their review, Lim et al. (2010) report that aerosol phase reactions of glyoxal with OH radicals performed under high initial concentrations tend to be faster and form more oligomers than non-radical reactions. They conclude that in clouds/fog conditions (i.e., diluted concentrations of 10^{-2}–1 mM), radical reactions yield organic acids, whereas in wet aerosols (i.e., concentrated conditions of 10 mM–10 M) they yield large multi-functional species, or oligomers, formed via radical–radical reactions. An oligomer is a molecule that consists of a few monomer units (from 2 to up to 30). Lim et al. (2010) and Tan et al. (2012) propose that radical–radical reactions to form oligomers are alkyl–alkyl radical additions, which always compete with O_2 addition reactions. This explains why oligomer formation is observed only at high initial precursor concentrations, inducing high alkyl radical concentrations (after initial OH-oxidation of the precursor) which are required for radical–radical reactions to take place in competition with the reaction of O_2. However, O_2 concentrations were supposed to stay constant at saturation (i.e., Henry's law equilibrium) in these studies, as they were only measured and the beginning and at the end of the reaction.

In the present study, in order to determine the atmospheric relevance of radical reactions, the radical mechanisms and the influence of O_2 concentrations on this chemistry is explored in details, using a different precursor, i.e., methyl vinyl ketone. This compound is an α,β-unsaturated carbonyl that is water soluble, it bears a highly reactive function (i.e., carbon-carbon double bond) that is likely to play a major role on radical chemistry and oligomer formation, as it was preliminarily shown by Liu et al. (2012). The reactivity of olefin compounds has been scarcely studied in the aqueous phase up to now, although a number of field measurements have observed them in atmospheric waters: unsaturated diacids were detected in rain and fog samples (7–14 % of the total mass of diacids: Kawamura and Ikushima, 1993; Sempéré and Kawamura, 1994; Kawamura et al., 1996) and in marine aerosols (2–7 % of the total mass of diacids; Fu et al., 2013). In clouds, it was observed that 1–18 % of the total mass of carbonyls were unsaturated carbonyls (among which methyl vinyl ketone) (van Pinxteren et al., 2005), and in biogenic aerosols, unsaturated polyols (C5-alkene-triols) represented 2–5 % of the total mass of identified polyols (Claeys et al., 2010). Finally, using NMR spectroscopy, Decesari et al. (2005) detected that 10–35 % (respectively 7–37 %) of the organic chemical functions were unsaturated in fog samples (respectively aerosols) in the Po Valley. In view of these numbers, one can reasonably suppose that 2–20 % of the organic matter concentration is unsaturated in atmospheric waters. Therefore, assuming total water soluble organic compounds (WSOC) concentrations of 0.01–1 µM in rain drops, 1–100 µM in cloud droplets, 1–100 mM in fog droplets and 1–10 M in wet aerosol, one obtains a range of unsaturated organic compounds of 0.0002–0.2 µM in rain drops, 0.02–20 µM in cloud droplets, 0.02–20 mM in fog droplets and 0.02–2 M in wet aerosol.

The aim of the present study was to determine the radical mechanisms involved in the oligomerization of MVK, and to identify the oligomers formed via this chemistry. MVK was used as a model compound for unsaturated organic compounds present in atmospheric waters, its initial concentrations were varied from 0.2 to 20 mM, thus representing the total concentrations of unsaturated organic compounds in fog droplet and wet aerosol. In order to determine the atmospheric relevance of this radical chemistry, the influence of temperature and dissolved oxygen concentrations were studied.

2 Experimental

A photoreactor was used to simulate the aqueous phase photooxidation of MVK. $HO^\bullet$ radicals were generated from H_2O_2 photolysis. In order to determine the reaction mechanism, a complete set of analytical strategies was used to identify the oligomers produced. Aqueous aliquots sampled at different photoreaction times were analyzed by mass spectrometry, UV absorbance spectroscopy and NMR. In order to test our radical mechanism for MVK oligomerization, its aqueous phase photooxidation was studied under various conditions of temperature, MVK initial concentrations, and above all, dissolved oxygen concentrations.

2.1 Photoreactor

The photoreactor set-up is based on the one described by Yao Liu et al. (2009) and Liu et al. (2012) with some modifications. It is a 450 cm^3 Pyrex thermostated photoreactor. The arc light source (LSH 601, Lot Oriel) is equipped with a 1000 W xenon arc lamp (LSB 551, Lot Oriel). A glass filter (ASTM 892 AM 1.5 standard) was used to remove the UV irradiation below 300 nm, resulting in an irradiance spectrum comparable to that of the sun at sea level, for a 48.3° zenith angle, but approximately twice more intense.

Compared to the set-up used by Yao Liu et al. (2009) and Liu et al. (2012), the photolysis rate constant of H_2O_2 increased by an order of magnitude due to the more powerful lamp used (Table 1). This resulted in higher $HO^\bullet$ concentrations using lower H_2O_2 initial concentrations, and thus led to faster MVK degradation and kept artifacts due to H_2O_2 reactivity to a minimum.

A 50 mL gas space was left over the liquid level. The loss of aqueous MVK to the gas phase was insignificant, based on its Henry's law constant (41 M atm^{-1} at 25 °C; Iraci et al., 1999) and on control experiments.

2.2 Experimental conditions

All experiments started with irradiation of UHQ water (18.2 MΩ cm, Millipore), then H_2O_2 (30 %, non-stabilized, Acros) was introduced, photolysed for 10 min until photostationary conditions were reached. MVK (99 %, Sigma Aldrich) was finally introduced at time noted 0 min. The experimental conditions (UV-visible irradiation, temperature, concentrations) were chosen in order to be representative of fog droplet and/or wet aerosol conditions. Additionally, a detailed study of the influence of oxygen initial concentrations was performed, in order to determine its role on radical chemistry, and its atmospheric relevance.

2.2.1 Control experiments

To check that the observed products resulted from the aqueous phase OH-oxidation of MVK, two control experiments were conducted: (1) MVK (20 mM) + H_2O_2 (400 mM) under dark conditions, and (2) direct photolysis of MVK (20 mM). MVK was not significantly consumed either in presence of H_2O_2 in the dark (1) or under direct irradiation (2). Additionally, we performed (3) direct photolysis of H_2O_2 (400 mM) in absence of MVK, and the observed decrease of H_2O_2 concentrations allowed us to determine its photolysis rate constant J (Table S1). We used UPLC-UV at 265 nm for H_2O_2 detection. The duration of these three control experiments was 300 min, consistent with the reaction time of the actual MVK photooxidation experiments.

2.2.2 Initial concentrations of reactants

Tan et al. (2010) have shown the important impact of initial concentrations on oligomer formation for α-dicarbonyls. The experiments were thus carried out with various MVK initial concentrations, i.e., 0.2 mM, 2 mM and 20 mM (corresponding to 9.6 to 960 mg C L^{-1}), which can be regarded as representative of the total concentrations of unsaturated organic compounds in fog droplet and wet aerosol (see Introduction).

The ratio $[H_2O_2]_0/[MVK]_0 = 20$ was chosen to favor $HO^\bullet$ reaction toward MVK over its reaction with H_2O_2 (Reaction R2, in Table S1) by more than 90 %. Under these conditions, $HO^\bullet$ concentrations were estimated to approximately 5×10^{-14} M, which fall in the range of the estimated values for cloud and fog droplets (Herrmann et al., 2010; Ervens and Volkamer, 2010).

2.2.3 Temperature, pH and dissolved oxygen

Temperature, pH and dissolved oxygen concentrations were continuously monitored in the solution using a Consort C3020 multi-parameter analyzer. Three relevant temperatures were tested, 5 °C, 9 °C and 25 °C. The pH of the unbuffered solution decreased from 6 to 3 within 90 min of photoreaction (Experiments A, B and C: $[MVK]_0 = 20$ mM, at 25 °C, 9 °C and 5 °C; Table 1).

At 25 °C, in experiments where dissolved oxygen concentrations were not constrained (Experiments A, B, C, E and F in Table 1), these concentrations were at Henry's law equilibrium with atmospheric O_2 in UHQ water. After H_2O_2 introduction the dissolved O_2 concentrations were supersaturated by a factor of 155 % (corresponding to 400 µM of O_2 in experiment A), due to H_2O_2 photooxidation (Reactions R3 and R4 in Table S1), and then they decreased down to nearly 0 during MVK photooxidation. Thus, for these experiments, O_2 was supersaturated (by a factor of 155 %) when MVK was introduced (called "supersaturated initial O_2 concentrations" experiments in the following). Due to this high variability, and also because oxygen is known as a radical polymerization inhibitor (Odian, 2004), the influence of initial dissolved oxygen concentrations were investigated.

To complete the investigation of the role of oxygen, we also performed experiments with low initial O_2 concentrations (experiments D) by bubbling a flow of argon in the solution before injecting MVK in order to evacuate as much O_2 as possible before the reaction started. Then the argon flow was stopped in order to prevent MVK from evaporation, and the samples were collected using a syringe through a septum to avoid atmospheric O_2 entering the reactor.

2.3 Mass spectrometric analyses of the solution

An ultra-high performance liquid chromatographic column coupled to a time of flight mass spectrometer equipped with a soft ionization electrospray source was used (Synapt-G2

Table 1. Experimental conditions of OH-oxidation of MVK, and comparison with our previous work, the study by Liu et al. (2012). In all studies, all experiments were unbuffered (free pH).

Exp. name/ Ref.	$[MVK]_0$ (mM)	$[H_2O_2]_0$ (mM)	O_2 conditions ($[O_2]_0$ µM, %)[a, b]	$[O_2]$ (µM) at Henry's law equilibrium[c]	Temp. (°C)	Lamp (W)	J (s^{-1})	$[HO^\bullet]$[d] (M)	τ_{life} (min)[e]	Analysis (number of experimental repetitions)
Liu et al. (2012)	20	1000	Supersaturated (1700, 659 %)[a]	258	25	300	7.5×10^{-7}	8.6×10^{-15}	262	HPLC-ESI-MS
A	20	400	Supersaturated (400, 155 %)[a]	258	25	1000	8.5×10^{-6}	4.3×10^{-14}	52	UPLC-ESI-MS (12) ESI-UHRMS (1) UV-spectroscopy (3) NMR-spectroscopy (1)
B	20	400	Supersaturated (580, 161 %)[a]	361	9	1000	8.5×10^{-6}	4.3×10^{-14}	52	UPLC-ESI-MS (1)
C	20	400	Supersaturated (656, 164 %)[a]	399	5	1000	8.5×10^{-6}	4.3×10^{-14}	52	UPLC-ESI-MS (4)
D	20	400	Low (60, 23 %)[b]	258	25	1000	8.5×10^{-6}	4.3×10^{-14}	52	UPLC-ESI-MS (4)
E	2	40	Supersaturated (320, 124 %)[a]	258	25	1000	8.5×10^{-6}	4.3×10^{-14}	52	UPLC-ESI-MS (2) UV-spectroscopy (1)
F	0.2	4	Supersaturated (280, 108 %)[a]	258	25	1000	8.5×10^{-6}	4.3×10^{-14}	52	UPLC-ESI-MS (2) UV-spectroscopy (1)

[a] Dissolved O_2 concentration at time 0 (i.e., MVK introduction), in presence of H_2O_2, surrounded by ambient air;
[b] Dissolved O_2 concentration at time 0, in presence of H_2O_2, after 30 min of argon flow bubbling into the solution;
[c] Theoretical $[O_2]$ (µM) at Henry's law equilibrium in ambient air before H_2O_2 addition from Benson and Krause (1984);
[d] The $HO^\bullet$ concentrations were calculated assuming the steady state approximation at time 0: $[OH] = \frac{2 \times J \times [H_2O_2]}{k_{MVK} \times [MVK] + k_2 \times [H_2O_2]}$
[e] MVK life time towards OH-oxidation: $\tau_{life} = \frac{1}{k_{MVK}[OH]}$

HDMS, Waters). It is noted UPLC-ESI-MS hereafter. This instrument enabled us to demonstrate the oligomerization dependence on oxygen, and to follow the oligomerization kinetics. One of the experiments A (at 25 °C, Table 1) was performed using an ultra-high resolution mass spectrometer coupled to an electrospray ionization source, noted ESI-UHRMS (LTQ-Orbitrap-XL, Thermo).

2.3.1 UPLC-ESI-MS analyses

Aqueous samples (taken from the photoreactor) were analyzed for organic species using Quadrupole-Time-of-Flight Mass Spectrometry and Ion Mobility Spectrometry (Synapt G2 HDMS, Waters, MA, USA) combined with electrospray ion (ESI) source and coupled with an Acquity UPLC system (Waters). The mass spectrometer was used in its resolution mode, up to 18 000 FWHM (Full width at half maximum) at 400 Da and allowed the determination of elemental composition of some organic species, using the I-FIT software. The I-FIT isotope predictive filtering is a strategy to reduce the number of proposed elemental compositions using algorithms to estimate the number of carbon, oxygen or sulfur atoms in an unknown molecule based on the mass of the molecular ion and the relative intensity of the 1st and 2nd isotopes (Hobby, 2005).

The chromatographic separations were carried out on a HSS T3 UPLC column (Waters Acquity High Strength Silica T3, 2.1 × 100 mm, 1.8 µM) at 40 °C. The mobile phases consisted in (A) 0.1 % formic acid in water (Fluka, 98 %) and (B) Acetonitrile (CAN; Optima LC-MS, Fischer). The gradient elution was performed at a flow rate of 600 µL min^{-1} using 5 to 95 % of B within 7 min and held at 95 % of B for 1.5 min. The sample injection volume was 10 µL.

The ESI source of this instrument contains two individual orthogonal sprays. One spray is for the column eluent, and the other one is for the internal standard called lock-mass. During each chromatographic run, leucine enkephalin (2 ng μL^{-1}, $C_{28}H_{37}N_5O_7$, MW 555.27, Waters Q-ToF product) was used for lock-mass correction to obtain accurate masses for each organic component eluting from the column. The lock-mass syringe pump was operated at 7 µL min^{-1}. A solution of sodium formate (CO_2HNa, Waters Q-ToF product) was infused daily in the ESI source to calibrate the instrument. Optimum ESI conditions were found using a 2.5 kV capillary voltage, 40 V sample cone voltage, 450 °C desolvation temperature, 120 °C source temperature, 20 L h^{-1} cone gas flow rate and 800 L h^{-1} desolvation gas flow rate. The ESI source has been optimized directly with the samples. These parameters allow increasing the signal to noise ratio, keeping soft ionization technique.

Data were collected from 50 to 1800 Da in the positive and negative ionization modes. All products were detected as their protonated molecules ($[M + H]^+$) or sodium adducts ($[M + Na]^+$) in the positive mode, and their deprotonated molecules ($[M - H]^-$) in the negative mode.

For experiments A (Table 1), complementary analyses were performed using MS/MS fragmentation to confirm the structure of the products. MS/MS experiments (below 200 Da) were carried out with a trap collision energy ramp

from 5 to 20 eV. Additionally, traveling wave ion mobility allowed us to separate ions which had the same elemental formula. The main parameters were the IMS Wave Velocity 650 m s^{-1} and the IMS Wave Height 40 V.

2.3.2 ESI-UHRMS analyses

One of the experiments A (at 25 °C, Table 1) was performed using an ultra-high resolution mass spectrometer coupled to an ESI source (LTQ-Orbitrap-XL, Thermo). Aqueous aliquots sampled from the photoreactor were diluted by a factor of 2 with ACN, and directly infused into the ESI at a 3 µL min^{-1} flow rate. Using a mixture (1 : 1) of ACN and aqueous samples helps the desolvation process in the ESI source, thereby ensuring more stable operations. ACN was chosen against methanol as this latter was shown to occasionally induce esterification during the ionization (Bateman et al., 2008). Each sample was measured in the negative and positive ionization modes, with the following optimized settings: source voltage – 3.5 kV; capillary temperature – 275 °C; tube lens voltage – 50 V in the positive mode; and source voltage – 3.7 kV; tube lens voltage – 90 V and same capillary temperature in the negative mode.

Transient acquisition time was set to 1 s, which corresponds to a nominal resolution of 100 000 at 400 Da, and to observe individual peaks resolution (FWHM) typically better than 200 000 at 200 Da. Each spectrum was obtained by averaging 20 min of acquisition time, so as to increase the S/N ratio of the lower intensity peaks. Acquisition was performed over two overlapping mass ranges: 50–300 Da and 150–1500 Da. This method overcomes transfer limitations of very wide mass ranges in the ion optics which guide the molecular ions through the LTQ to the Orbitrap mass analyzer.

External mass calibration was made daily by infusing a calibration mixture (L-methionine-arginyl-phenylalanyl-alanine, caffeine, and ultramark: MSCAL 5-10EA Supelco) having peaks in the range 195 to 1921 Da. The obtained mass accuracy was as low as 2–5 ppm, and better for peaks with a relative intensity above 0.5 % (Makarov et al., 2006).

For our moderately complex mixture (∼ 6000 peaks), containing only O, C, H, and Na, unambiguous elemental formula assignments were established below 350 Da within 1 mDa using a custom computer software (Attributor v1.05) developed by Orthous-Daunay (2011) and described in Danger et al. (2013). It is based on a suite of scripts that allow to evaluate the most probable attribution of a high resolution peak, based on its mass, the presence and relative intensity of isotopic peaks, as well as chemical rules (nitrogen rule, even electron ions, etc.) Using a Kendrick analysis (Hughey et al., 2001) based on the MVK pattern (i.e., C_4H_6O) found by Liu et al. (2012) and on the unambiguous attribution of most peaks below 350 Da, series of regularly spaced peaks were identified in the spectrum, and used to extend the formula attribution toward higher masses. This extension into Kendrick series was also checked against isotopic patterns. Typical standard deviation of the Kendrick mass defect in any such identified series was lower than 0.5 mDa, which ensures the proper attribution of all the members of a series to within less than 1 mDa in the full mass range explored (i.e., 50–1500 Da).

2.4 Spectroscopic analyses of the solution

2.4.1 UV Spectroscopy

UV absorption spectroscopy (Agilent 8453) was used in a wavelength range from 190 to 400 nm to monitor MVK concentrations and chemical structure changes during the reaction. Diluted in water, MVK shows, like all α,β-unsaturated ketones (Yadav, 2012), an intense absorption band (K-band; $\pi \rightarrow \pi^*$ transition) at 211 nm ($\varepsilon_{211} = 7692\,M^{-1}\,cm^{-1}$) and a weak absorption band (R-band; $n \rightarrow \pi^*$ transition) at 296 nm ($\varepsilon_{296} = 30\,M^{-1}\,cm^{-1}$). Because the absorbance of H_2O_2 below 240 nm is intense (i.e., $\varepsilon_{211} = 100\,M^{-1}\,cm^{-1}$), it was interfering with the $\pi \rightarrow \pi^*$ transition of MVK under our experimental conditions, where $\frac{[H_2O_2]_0}{[MVK]_0} = 20$.

A volume of catalase from bovine liver (C 3155, Sigma Aldrich) was added to each sample to quench efficiently the H_2O_2 absorbance signal within a few minutes (Li and Schellhorn, 2007).

2.4.2 NMR spectroscopy

One of the experiments A was analyzed using NMR spectroscopy (Table 1). The instrument used was a Bruker Avance 500 MHz equipped with a 5 mm inverse-triple tuned (TXI) $^1H/^{13}C/^{15}N$ with z gradient coil probe. For 1-D ^1H-Spectra, 128 scans were collected with an impulsion time of 7.5 µs, a relaxation delay of 5 s, an acquisition time of 4.67 s, a spectral window of 5000 Hz and 64 K data points zero filled to 128 K before Fourier transformation with 0.3 Hz line broadening. For 2-D homonuclear (COSY and TOCSY) and heteronuclear ($^1H/^{13}C$ HSQC and HMBC) experiments were performed with quadrature phase detection in both dimensions, using state-TPPI or QF detection mode in the indirect one. For each 256 (homonuclear experiments) or 512 (heteronuclear experiments) increments in the indirect dimension, 2 K data points were collected and 16 or 32 transients were accumulated in the direct dimension. ^{13}C decoupling (GARP) was performed during acquisition time for heteronuclear experiments. A $\pi/2$ shifted square sine-bell function was applied in the indirect dimension before Fourier transformation. Spectra were treated with Topspin version 2.0. All NMR spectra were recorded at 25 °C.

Aliquots of 540 µL of the aqueous solution sampled from the photoreactor (at 5, 10, 25, 70 and 90 min of reaction) was supplemented with 60 µL of a buffer containing 100 mM phosphate and 5 mM of sodium tetra deuterated trimethylsilyl propionate ($TSPd_4$, Eurisotop). $TSPd_4$

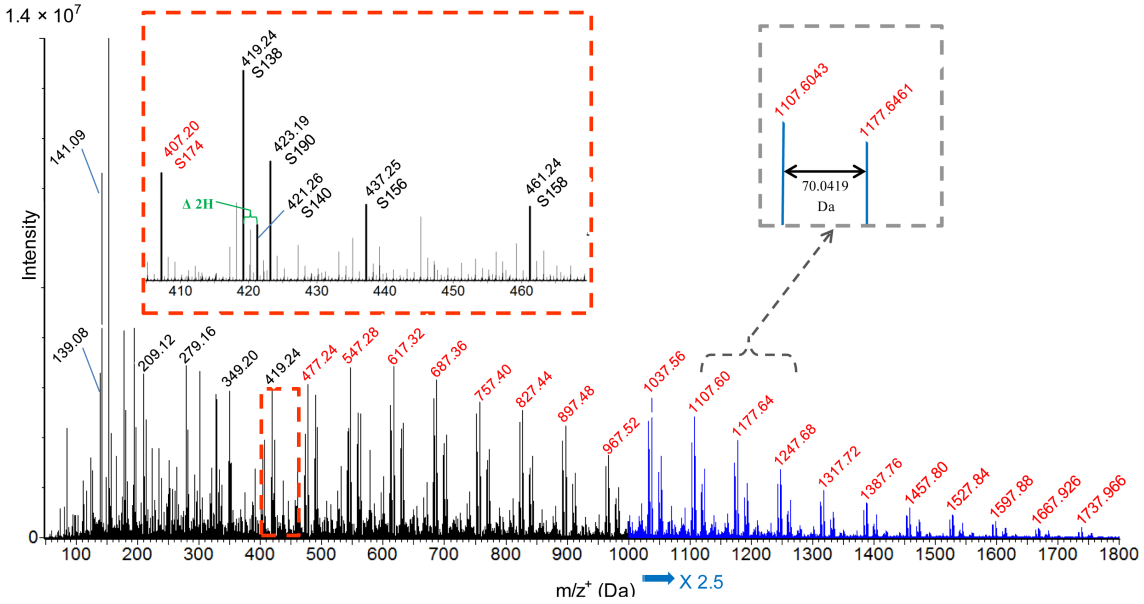

Fig. 1. Mass spectrum (obtained using UPLC-ESI-MS from 0 to 1800 Da) for the retention time range 0 to 7 min, in the positive mode, at $t = 50$ min of experiment C. The most intense series (S174) is highlighted in red. Each group of peaks represents a degree of polymerization (DP). Left zoom: main series detected for DP = 4. Right zoom: MVK regular pattern of mass differences of 70.0419 Da. Another regular pattern of mass difference of 2.0157 Da corresponding to 2 H is also observed (in green in the left zoom).

constituted a reference for chemical shifts (0 ppm) and quantification. Final volumes of 600 µL of prepared samples were put in 5 mm-diameter NMR tubes.

Additionally, an aliquot of 5 mL sampled at the end of the kinetic (90 min of reaction) was freeze-dried, re-suspended in 600 µL of $CDCl_3$ and transferred in a 5 mm NMR tube for further 1-D and 2-D NMR analysis. D_2O and $CDCl_3$ were used for locking and shimming.

3 Results and discussions

3.1 Evidence for the formation of oligomers by radical oligomerization of MVK

The aqueous phase OH-oxidation of MVK leads to the formation of series of oligomers as indicated by the analyses of our solutions, and is in good agreement with the study by Liu et al. (2012). Furthermore, the whole set of analyses showed that the produced oligomers were formed by radical oligomerization of MVK, as discussed below. The ionic oligomerization of MVK (through carbocations or carbanions) was unlikely under our experimental conditions because the protic and nucleophilic characters of the solvent (water) inhibit oligomerization by reacting instantly with carbocation and carbanion initiators (Odian, 2004).

3.1.1 Series of oligomers evidenced by mass spectrometry and NMR spectroscopy

Figure 1 shows a mass spectrum (obtained using UPLC-ESI-MS) for the retention time range 0–7 min, recorded in the positive mode, at 50 min of MVK photooxidation at 5 °C (experiment C in Table 1). Spectra typically contain hundreds of peaks in both modes, and it was out of the scope of this study to explore their full complexity. Yet, oligomer systems are clearly visible, with very regular spacing of 70.0419 Da, which correspond to the exact mass of the precursor, MVK, as confirmed by the ESI-UHRMS analysis. These systems extend up to 1800 Da, thus containing up to 25 monomers. Using a lower intensity xenon lamp, and a lower resolution mass spectrometer (Table 1), Liu et al. (2012) also found oligomer series at the same nominal masses, with slightly different intensities. The main differences observed here were the kinetics. The maximum intensity was reached around 50 min here at 25 °C, instead of 20 h previously (Liu et al., 2012) at the same temperature, certainly due to the higher $HO^{\bullet}$ concentrations obtained here with a more powerful irradiation lamp (Table 1).

Experiment A was repeated 12 times and analyzed using the same UPLC-ESI-MS conditions. The exact masses measured for the oligomers were very repeatable, as was the kinetics of their appearance and of MVK consumption.

Experiment A was also monitored once using ^{1}H NMR spectroscopy (Table 1). Figure 2 shows ^{1}H NMR peaks resonating at 2.36 ppm (s), 6.13 ppm (dd), 6.37 ppm (m) and

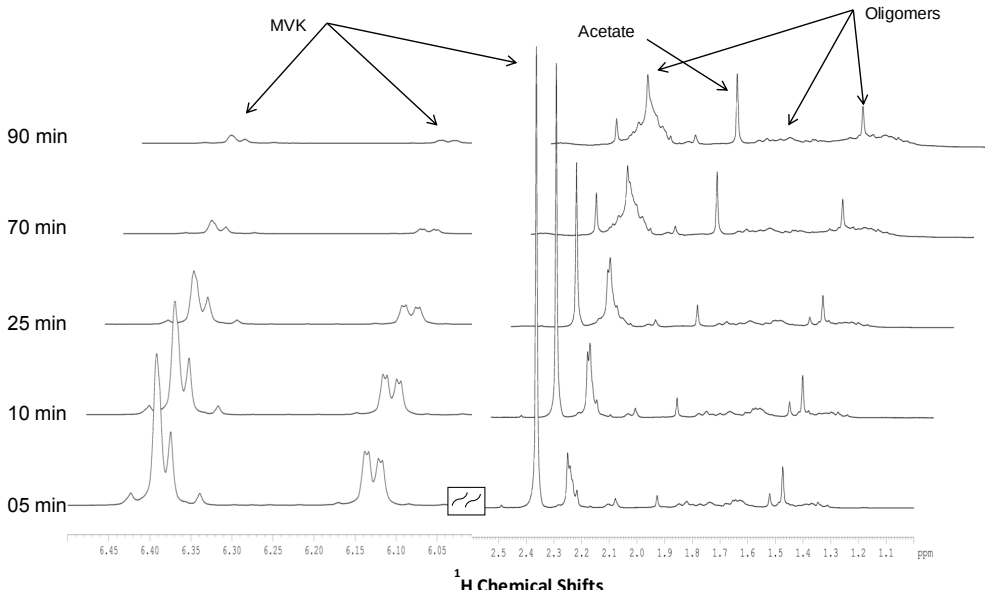

Fig. 2. Monitoring experiment A by 1-D ^{1}H NMR (recorded in phosphate buffer containing 10 % D_2O). The intensities of oligomer structures increase with time, to the detriment of MVK.

6.39 ppm (m) that were assigned to the ^{1}H of MVK. These ^{1}H peaks decreased with time while new ^{1}H NMR signals resonating at 1.15–1.88 ppm and 2.13–2.34 ppm increased with time, indicating the formation of reaction products, to the detriment of MVK. These signals are very wide and are consistent with the presence of overlapping signals due to a variety of oligomers (Alarifi and Aouak, 2009; Ziaee et al., 2009). Overall, both mass spectrometry and NMR measurements indicate that a wide variety of oligomers was formed from the reactivity of MVK and that this formation of high mass oligomers occurs through an extremely fast mechanism, as in radical propagation systems.

3.1.2 Indications on the chemical structure of the monomers according to NMR and UV-spectroscopic measurements

In order to identify the structure of the oligomers observed by ^{1}H NMR spectroscopy in Fig. 2, the sample taken at the end of the reaction (experiment A at 90 min) was freeze-dried and re-suspended in $CDCl_3$ leading to a concentrated solution of the oligomers allowing the measurement of 1-D and 2-D NMR spectra (Fig. 3). The analysis of the ^{1}H NMR resonances in the 1-D ^{1}H NMR spectrum (Fig. 3a) and of the $^1J^1$H-^{13}C correlations present on the 2-D ^{1}H-^{13}C HSQC NMR spectrum (Fig. 3b) allowed proposing assignments of CH, CH_2 and CH_3 functional groups of the putative oligomeric structure shown in Fig. 3. Long range J_{1H-13C} correlations observed on the 2-D ^{1}H-^{13}C HMQC NMR spectrum (Fig. 3c) clearly demonstrated the presence of C=O functional groups belonging to the proposed oligomeric structure. NMR experiments also showed that MVK was largely converted into oligomer forms and that most of the signals of C=C bonds have disappeared at 70 and 90 min of reaction, thus indicating that the oligomers are mostly aliphatic.

Using UV absorption spectroscopy from 190 to 400 nm during experiment A, the evolution of the two intense absorption bands of MVK are shown in Fig. 4. During the photooxidation process, the $n \rightarrow \pi^*$ transition (Fig. 4a) was clearly shifted to shorter wavelengths (blue shift; i.e., from 296 nm at time 0 to 269 nm at 90 min of reaction), with increasing absorption intensity. The $\pi \rightarrow \pi^*$ transition did not show any shift (in the range of the investigated wavelengths) (Fig. 4b), but a clear decrease of its intensity (at 211 nm) was observed. The observed blue shift shows that, in the reaction products formed, the corresponding transition needs higher energy (than in MVK) to get excited (i.e., at shorter wavelengths). This can be due to the loss of the conjugation, probably due to the loss of the vinyl function, in good agreement with the NMR analyses. Furthermore, the absorption intensity at 211 nm was directly proportional to the MVK concentrations during the reaction, as it was verified with ^{1}H NMR (at 2.36 ppm) and with mass spectrometry.

3.1.3 Time profiles of MVK, and reaction products

The observed kinetics of the MVK degradation (Fig. 5) were characteristic of those of the monomers in radical polymerization (Pearce et al., 1982). During the initiation step of the reaction ($\sim$ 13 min at 25 °C), MVK was slowly degraded, and low molecular weight reaction products were formed, such as acetate as observed by 1-D ^{1}H NMR (at 1.90 ppm, Fig. 2). More generally, organic acids were produced, as denoted by

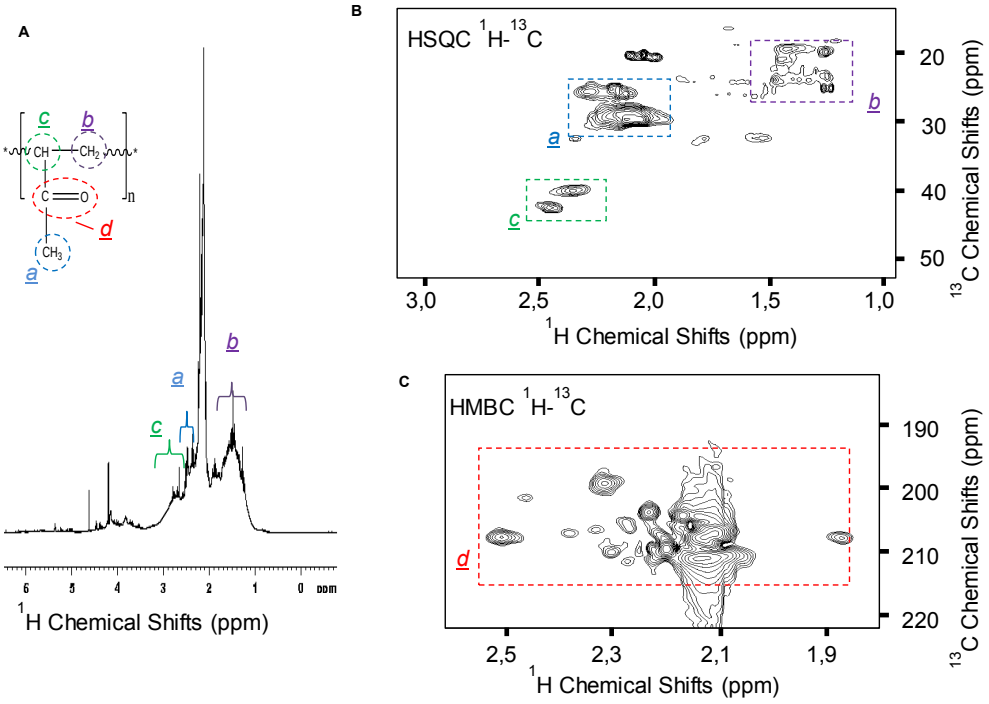

Fig. 3. Proposed structure identification of oligomers. 1-D ^{1}H NMR spectrum **(A)** and 2-D ^{1}H-^{13}C NMR spectra (**B** and **C**) of a sample taken at 90 min of reaction during experiment A, freeze-dried and re-suspended in $CDCl_3$.

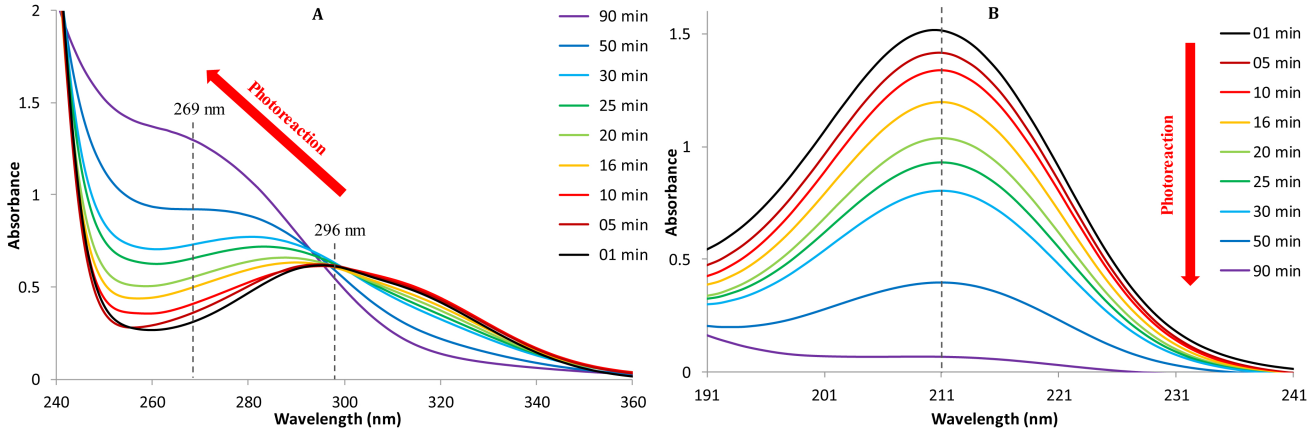

Fig. 4. UV absorption spectra of the solutions sampled during experiment A (with catalase added prior to analysis), **(A)**: from 240 to 360 nm; and **(B)**: diluted by 100 from 191 to 241 nm.

the fast decrease of the pH, from 6 to 4, during this step. After 13 min, oligomerization started, and the kinetics of MVK degradation significantly increased (Fig. 5). The maximum of oligomers intensity was reached at 50 min of reaction, for the major series. After 90 min of reaction, more than 95 % of MVK was consumed and the oligomers started to decrease.

3.1.4 Comparison of the oligomers formed by OH-oxidation of MVK with a synthetic oligomer of MVK

In order to confirm the radical MVK oligomerization during OH-oxidation, oligomers of MVK were synthesized using a water-soluble radical initiator (V50: 2,2'-Azobis(2-methylpropionamidine) dihydrochloride, Wako) which forms two symmetric radicals by thermal homolysis (Reaction 6 in Supplement Table S2), under oxygen-free conditions at $T \geq 50\,^{\circ}C$ and similar initial concentrations

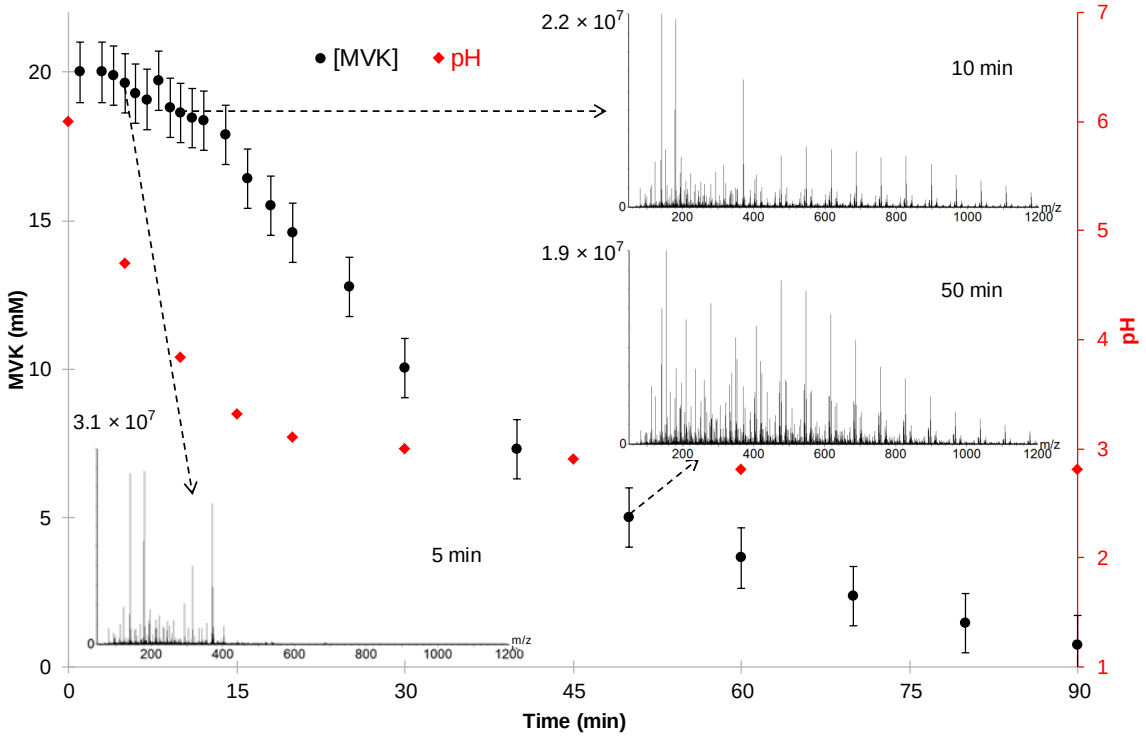

Fig. 5. MVK time profile (as measured by UV Spectroscopy) and mass spectra (obtained using UPLC-ESI-MS for the retention time range 0–5 min in the positive mode) at 5, 10 and 50 min of reaction, during experiment A (MVK 20 mM, 25 °C, under supersaturated O_2 initial conditions).

of MVK as in our photooxidation experiments (Table S2). $[MVK]_0/[V50]_0$ ratio was kept constant at 80 (Table S2) and UV absorption spectra were monitored at the beginning ($t = 0$ min) and after the reaction ($t = 120$ min).

UV absorption spectra obtained during the OH-oxidation of MVK in the aqueous phase (Fig. 4) and after the synthesis of MVK oligomers in the aqueous phase (Fig. S1) both showed the same blue shift on the $n \rightarrow \pi^*$ transition band (from 296 nm), and a significant decrease of the intensity at 211 nm.

The mass spectra obtained for the synthesized oligomer (Fig. S2) were very similar to those obtained during the OH-oxidation of MVK in the aqueous phase (Fig. 1). Figure S2 shows very regular spacing of 70.0419 Da, and a Poisson distribution, typical of polymers (Pearce et al., 1982). Additionally, the method used to identify the initiator radicals (see Sect. 3.2 below), applied to the high resolution mass spectrum obtained from the synthesized oligomers, allowed us to determine the chemical formula of the initiator radical formed from the V50 molecule (Reactions 6 and 7 in Supplement Table S2).

Overall, this comparison confirms the radical character of the MVK oligomerization during its OH-oxidation in the aqueous phase under similar conditions.

3.2 Proposed mechanism of radical oligomerization of MVK

In view of the observations performed in Sect. 3.1, we proposed a simple chemical mechanism of radical oligomerization of MVK that is likely to occur during its OH-oxidation in the aqueous phase (Fig. 6). In the initiation step, the reactivity of MVK towards the $HO^\bullet$ radical yields (directly or indirectly: see below Sect. 3.4) initiator radicals $iR^\bullet$ (Odian, 2004). Each radical adds on another MVK molecule by opening its vinyl double bond, leading to the formation of another radical, iR-MVK$^\bullet$ which can then add to another MVK molecule in the same way, and so on, leading to the formation of a large radical, iR-$(MVK)_n$-MVK$^\bullet$. The propagation keeps on increasing the chain length, until the radical termination. Termination occurs by bimolecular reaction between two radicals, by coupling or by disproportionation (Fig. 6), thus yielding, for each initiator radical $iR^\bullet$, two oligomer series including one saturated and one unsaturated terminal group (Gibian and Corley, 1973).

This chemical mechanism is in very good agreement with our experimental observations. The regular mass spacing of 70.0419 Da observed in mass spectra (Fig. 1) corresponds exactly to the mass of the monomer MVK in the mechanism. Radical oligomerization is in good agreement with a very fast propagation with prompt growth of the chain

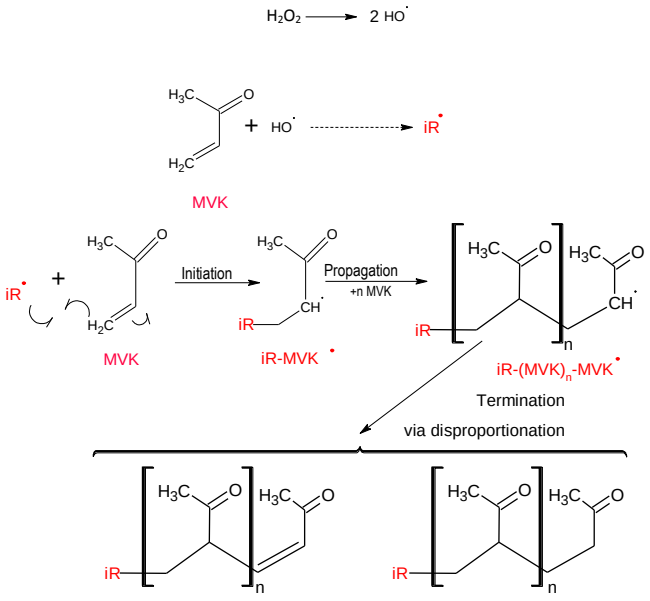

Fig. 6. Scheme of the proposed mechanism of radical oligomerization of MVK in the aqueous phase, initiated by OH-oxidation. iR$^{\bullet}$ is an initiator radical; MVK is the monomer or the repeating unit, n is the degree of polymerization. For clarity, only the external radical additions are shown.

to high molecular weight oligomers after an initiation step (Fig. 5). The MVK oligomerization is in good agreement with the significant loss of the vinyl group observed in Figs. 2 and 3, which is correlated with a significant loss of double bond conjugation as observed in Fig. 4. Additionally, this is in agreement with the fact that oligomerization of carbon–carbon double bonds is by far more likely than carbonyl groups because of the polarized nature of the latter (Odian, 2004).

Finally, the termination step of the mechanism is in good agreement with the observation of the same degree of polymerization (DP) (i.e., $n =$ number of monomers) for series of oligomers in mass spectra distant by 2.0156 Da (Fig. 1).

The scheme of the proposed mechanism (Fig. 6) only shows radical additions on the β-carbon of MVK for clarity. Although both α-β-additions are possible at each step, β-additions are likely favored because resonance with the carbonyl group gives it a stronger positive character. These additions lead to the formation of a number of isomers that grows exponentially with the DP. This is clearly observed in Fig. S3 showing the extracted UPLC-ESI-MS chromatogram of one of the most intense series of oligomers R-OH-(MVK)$_n$ (S174 colored in red in Fig. 1) formed during OH-oxidation of MVK after 50 min of reaction. The retention time of the oligomers regularly increases with the DP, certainly due to the growth of the corresponding molecules. Additionally, the width of the chromatographic peaks increases with the DP (from $n = 1$ to $n = 5$) unambiguously indicating that there are different products at the same mass, probably because of different tacticities of oligomers. After $n = 5$, the peaks become sharper and their area decreases, indicating that one way of oligomerization may be privileged due to steric hindrance for example. In this series, which is one of the most intense ones, oligomers with a DP up to 23 ($n = 23$) were detected.

3.3 Effects of initial conditions on the oligomer formation

The parameters varied, oxygen concentrations, temperature and MVK initial concentrations were chosen because they are known to significantly influence radical polymerization (Odian, 2004). A second reason for testing the influence of the initial concentrations of MVK was that organic concentrations can vary by orders of magnitude in the atmosphere from cloud droplet to wet aerosol (see Introduction).

Dissolved O_2 is known as a major inhibitor of radical polymerization, and also atmospheric dissolved O_2 concentrations in the condensed phase are not known, but are supposed to be saturated. Temperature is known to influence not only the kinetics of the reactions but also the oxygen Henry's law equilibrium (Table 1). The results of these experiments allowed us to confirm the mechanism of radical oligomerization of MVK, and also to identify a number of radical initiators (Sect. 3.4).

3.3.1 Effect of initial concentrations of MVK

Between experiments A, E and F (Table 1), initial concentrations of MVK varied from 20 to 0.2 mM with identical temperature (25 °C) and similar initial dissolved O_2 concentration (supersaturated). These three experiments show that different initial concentrations of MVK induced important effects on the oligomer formation, as observed by UPLC-ESI-MS (Fig. 7). The same major series of oligomers were observed at the three initial concentrations, but the chain length increased with the initial MVK concentration. For example, for the series depicted in red in Fig. 1 and in Fig. 7, the observed DP was 23 at 20 mM initial MVK concentration, 9 at 2 mM, and 4 at 0.2 mM. This correlation between the DP and the initial concentration of MVK is in very good agreement with the kinetic chain length of a radical chain oligomerization (Odian, 2004).

Finally, Fig. 7 clearly shows that for the high initial MVK concentrations (2 and 20 mM), the main reaction products were the oligomers (up to 800 and 1800 Da, respectively), while at the low initial MVK concentration studied (0.2 mM), low molecular weight reaction products were mainly formed (up to 230 Da). It is probable that at the latter initial concentration, the observed formation of initiators recombined because the MVK concentration was too low to propagate the radical oligomerization to higher chain lengths.

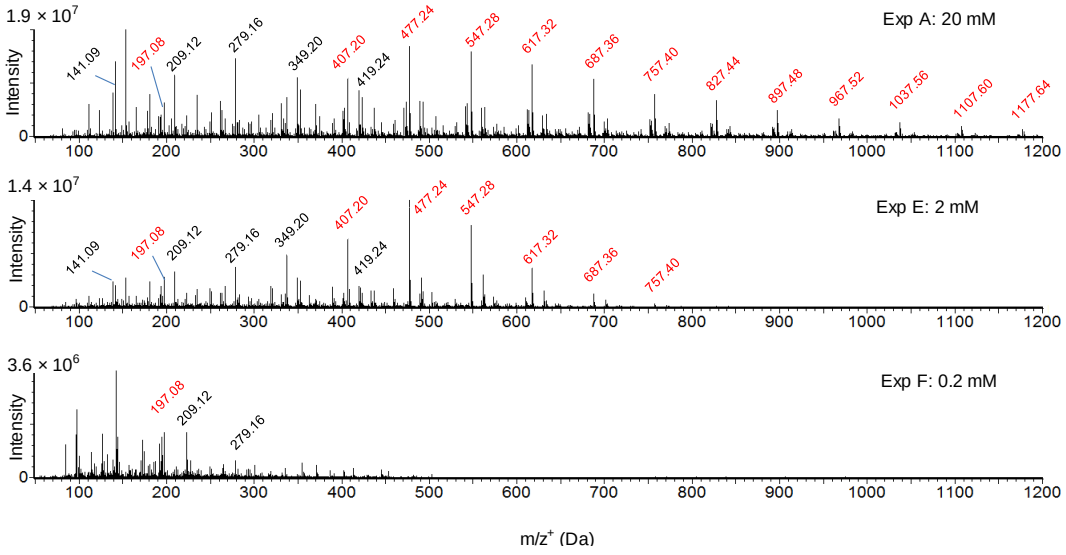

Fig. 7. Mass spectra (obtained using UPLC-ESI-MS, for the retention time range 0–5 min, in the positive mode) during experiments A, E and F (i.e., at 25 °C, for different initial MVK concentrations and at different reaction times (corresponding to the maximum oligomers intensity): 5 min for 0.2 mM; 15 min for 2 mM and 50 min for 20 mM. The most intense series (S174) is highlighted in red, as in Fig. 1).

3.3.2 Effects of initial concentrations of dissolved oxygen and temperature

Experiments A and D (Table 1) were performed under the same initial concentrations of MVK (20 mM) and temperature (25 °C), with very different initial dissolved O_2 concentrations: supersaturated and low initial O_2 concentrations, respectively, i.e., higher and lower than Henry's law equilibrium (by a factor of 1.7 and 4.5, respectively; Table 1). The results showed that the initial dissolved O_2 concentrations had a drastic effect on oligomerization, and on the kinetics of MVK consumption, in very good agreement with a mechanism of radical oligomerization of MVK. Dissolved O_2 is known to inhibit free radical photo-oligomerization by reacting with radical species to form chain terminating oxygenated compounds such as hydroperoxides (Decker and Jenkins, 1985). In our experiments, a strong inhibition of the oligomer formation by 155 % supersaturated dissolved O_2 was observed (Fig. 8a): at low initial O_2 concentrations (experiment D), the whole oligomer series developed within 5 min of reaction, while only first elements of the series appeared at the same reaction time under "supersaturated initial O_2 concentrations" (experiment A). This phenomenon, which was observed for all the other series of oligomers, shows that the reactivity of the initiator radicals ($iR^\bullet$) underwent a competition kinetic between their reaction towards O_2 and towards MVK for further oligomerization propagation. When O_2 was present, $iR^\bullet$ consumed O_2 very rapidly (i.e., faster than O_2 renewal from the gas phase and from H_2O_2 reactivity), and when O_2 concentration was sufficiently low, the competition furthered the oligomerization pathway which was extremely fast. Figure 9 shows a very contrasting behavior of MVK time profiles between "low initial O_2 concentrations" and "supersaturated initial O_2 concentrations" conditions. Under "supersaturated initial O_2 concentrations", two kinetic steps were observed: a slow one during which the oligomers were poorly formed, followed by a fast one where oligomers were actively formed (Figs. 5 and 9b). In contrast, under "low initial O_2 concentrations", the kinetic of MVK consumption was fast from the beginning (only one step was observed), and oligomerization started as soon as MVK was introduced (Figs. 9a and 8).

Figure 9 also shows the behavior of dissolved O_2 under three different conditions (experiments D, A and C). For all of these conditions, before the injection of H_2O_2, dissolved O_2 was at its Henry's law equilibrium with ambient O_2 in the gas phase. When H_2O_2 was added, dissolved O_2 concentrations increased due to the self reaction of $HO_2^\bullet$ and/or $O_2^{\bullet-}$ radicals in the aqueous phase (see Reactions R3 and R4 in Table S1). Then, as soon as MVK was introduced, the time profiles of O_2 concentration followed those of MVK, thus indicating that O_2 reacted with the radicals formed from MVK, even when oligomerization was the dominant pathway. Interestingly, under "supersaturated initial O_2 concentrations", the oligomerization acceleration started when O_2 concentrations were depleted from their initial values, but still they were higher than their Henry's law equilibrium (by a factor of 120 % and 140 % at 25 and 5 °C, respectively), thus showing the atmospheric relevance of these oligomerization processes (see atmospheric implications).

Experiments A, B and C differ for the temperature (i.e., 25 °C, 9 °C and 5 °C) with identical initial concentrations of MVK (20 mM) and similar dissolved O_2 concentration (supersaturated). The kinetic decay of MVK was clearly

Table 2. Oligomer series identified by UPLC-ESI-MS and ESI-UHRMS in positive and negative modes.

Series		iR-$(MVK)_{n=1}$		$\Delta_{intensity}$[d]
Name[a]	Formulas[b]	Formulas[c]	m/z (Da)[c]	
S138	MVK-$(MVK)_n$	$[C_8H_{10}O_2, +H]^+$	139.0759	+13 %
S140		$[C_8H_{12}O_2, +H]^+$	141.0916	+30 %
S156	R-$(MVK)_n$	$[C_8H_{12}O_3, +H]^+$	157.0865	+12 %
S158		$[C_8H_{14}O_3, +Na]^+$	181.0841	+10 %
S154	MVK-OH-$(MVK)_n$	$[C_8H_{10}O_3, -H]^-$	153.0552	−19 %
S156'		$[C_8H_{12}O_3, -H]^-$	155.0708	−6 %
S190	R-$(MVK)_n$-OOH	$[C_8H_{14}O_5, +Na]^+$	213.0739	−6 %
S172	R-OH-$(MVK)_n$	$[C_8H_{12}O_4, -H]^-$	171.0657	−16 %
S174		$[C_8H_{14}O_4, +Na]^+$	197.0814	−2 %
S128	(Acetic acid)-$(MVK)_n$	$[C_6H_8O_3, -H]^-$	127.0395	−39 %
S130		$[C_6H_{10}O_3, -H]^-$	129.0552	−17 %
S140'	(Methylglyoxal)-$(MVK)_n$	$[C_7H_8O_3, -H]^-$	139.0395	−28 %
S142		$[C_7H_{10}O_3, -H]^-$	141.0552	−12 %

[a] For each series, the name is given by "S" followed by a number corresponding to the nominal mass of the first oligomer, i.e., iR-$(MVK)n = 1$.

[b] The chemical structures are given in Fig. 10. R$^\bullet$ corresponds to the radical:

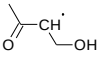

[c] Ions (and corresponding m/z) identified by UPLC-ESI-MS and/or ESI-UHRMS in experiment A;

[d] Intensity ratio of the series after 50 min of OH-oxidation of MVK (20 mM):

$\Delta_{intensity} = \frac{TSI_{Low\,O_2} - TSI_{supersaturated\,O_2}}{TSI_{supersaturated\,O_2}}$, with: TSI = total Series' intensity

influenced by the temperature during the initial step (Fig. 9b and c). Additionally, the lower temperature induced higher initial dissolved O_2 concentrations, and both these phenomena explain the time delay of the acceleration of oligomerization at 5 °C compared to 25 °C (at around 25 and 13 min, respectively). In contrast, the fast decay of MVK was not influenced by the temperature, thus showing that the radical mechanism of oligomerization of MVK at 20 mM is the dominant pathway for MVK consumption at this step, and it has a very small activation energy.

Finally, when most of the MVK was consumed, all oligomer series reached their maximum intensities, with slight differences from one condition to the other as illustrated for one series in Fig. 8b. These slight differences are particularly interesting to investigate the comprehension of the initial steps of the radical mechanism.

3.4 Identification of oligomers and their initiator radicals

In Fig. 10, starting from the known mechanism of OH-oxidation of MVK in the aqueous phase (Liu, 2011; Zhang et al., 2010; Huang et al., 2011), the possible oligomerization developments were added according to the experimental observations discussed above. The chemical structures of the identified oligomers are shown in Fig. 10 as well as their series names. The latter are also reported in Table 2 together with the corresponding m/z and chemical formulas obtained for the first oligomer ($n = 1$) of each series (i.e., iR-$(MVK)_{n=1}$) by UPLC-ESI-MS and ESI-UHRMS analyses. The identification was performed on the smallest oligomer of each series because the resolution and sensitivity of both instruments are optimum for $100 < m/z < 350$ Da. The identifications of the most intense peaks were further confirmed by MS/MS analyses. This method of identification, applied to the synthetic oligomers of MVK formed from the V-50 initiator, allowed us to identify the most intense series of oligomers as the one shown in Reaction (R7) (in Supplement Table S2), thus showing the robustness of the method. The identification of the longer chain oligomers ($n \geq 2$) was further completed by the Kendrick analysis based on the MVK (C_4H_6O) pattern, using the method mentioned in Sect. 2.3.

The oligomers were likely formed according to the mechanism shown in Fig. 6, each one being initiated by an initiator radical iR$^\bullet$ formed from the OH-oxidation of MVK (Fig. 10). The OH-oxidation of MVK proceeds via OH-addition (1a) and H-abstraction (1b). For clarity, only OH-addition on the β-carbon of MVK is fully developed in Fig. 10, as it is more likely than α-addition, due to resonance with the carbonyl group, and steric hindrance. Furthermore, both β-and α-additions lead to isomeric forms of oligomers with the

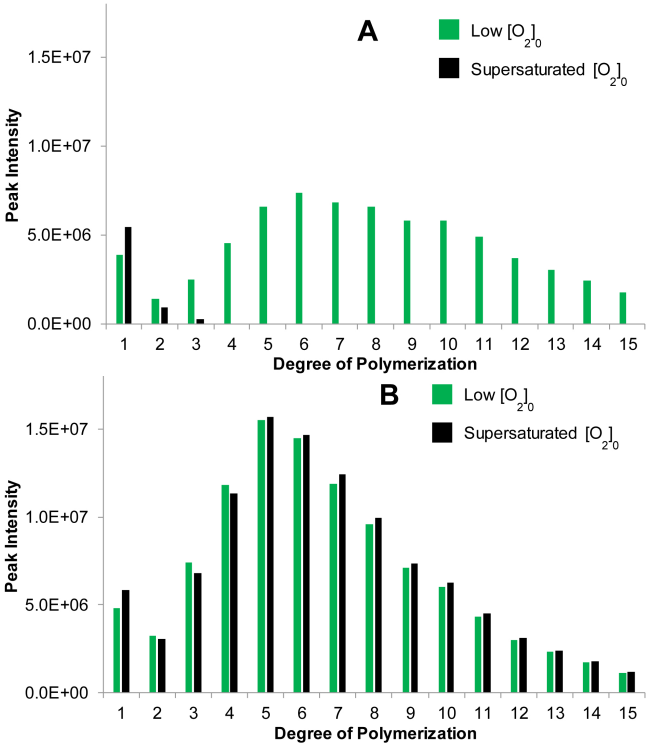

Fig. 8. Effect of initial O_2 concentrations on the oligomer series S174 up to 1200 Da (obtained using UPLC-ESI-MS, for the retention time range 0–5 min, in the positive mode) after **(A)** 5 min and **(B)** 50 min of OH-oxidation of MVK (20 mM) in the aqueous phase at 25 °C, under initial low O_2 conditions (in green: $[O_2]_0 = 60\,\mu M$), and under initial supersaturated O_2 conditions (in black: $[O_2]_0 = 400\,\mu M$).

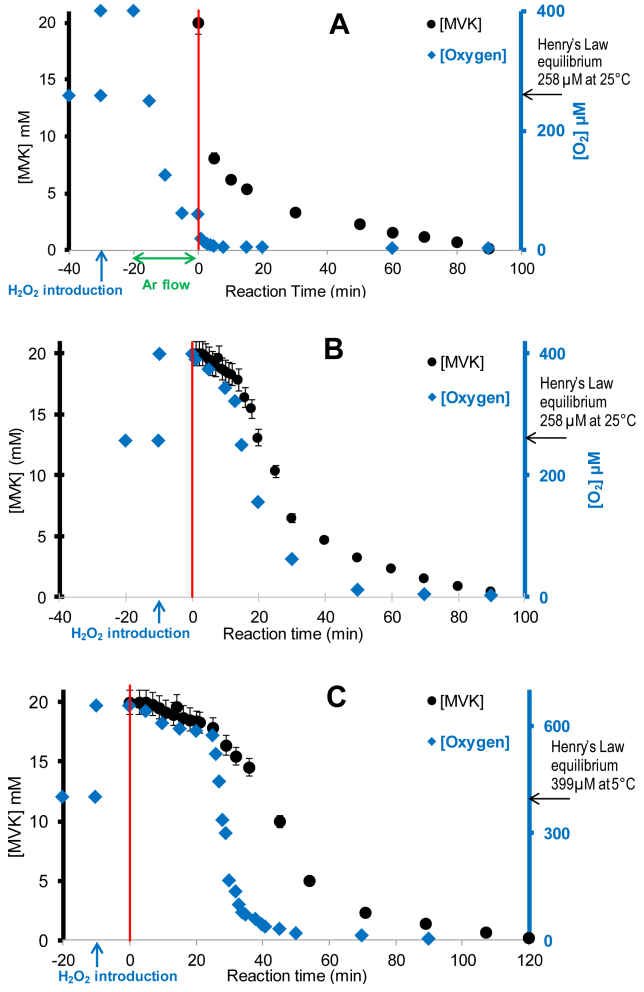

Fig. 9. Time profile of MVK and dissolved O_2 concentrations under different temperature and initial O_2 concentrations: **A)** experiment D (25 °C, under low initial O_2 concentration: 60 µM); **(B)** experiment A (25 °C, under supersaturated initial O_2 concentration: 400 µM); **(C)** experiment C (5 °C, under supersaturated initial O_2 concentration: 400 µM). Time 0 = MVK introduction (red line).

same masses which could not be discerned by mass spectrometry. In the proposed mechanism, each step leads to the formation of a radical iR$^\bullet$, which undergoes either O_2 addition or oligomerization with MVK, in good agreement with our experimental observations. A detailed description of the mechanism is shown for pathways 1a and 1b (Fig. 10).

3.4.1 Pathway 1a

OH-addition leads to the formation of radical R$^\bullet$, which undergoes either oligomerization with MVK (2a) or O_2 addition (2b). Pathway 2a leads to the formation of radicals R-(MVK)$^\bullet_n$ which terminate either directly to form R-(MVK)$_n$ (i.e., series S156 and S158) via the disproportionation mechanism indicated in Fig. 6 or after O_2 addition (3a) followed by H-abstraction (on $HO_2^\bullet$, MVK or an oligomer) to form hydroperoxides R-(MVK)$_n$-OOH (series S190) (Decker and Jenkins, 1985). An isomer of the latter oligomer series (S190) may also be produced from the oligomerization of ROO$^\bullet$ radicals, which proceeds via the disproportionation mechanism (Fig. 6). However, this pathway (not shown) is of minor importance because the corresponding unsaturated series (S188) showed a very weak signal by both mass spectrometers (below 1/100 of the most intense series shown in Table 2). ROO$^\bullet$ radicals can also undergo self reaction (4a) leading to a tetroxide which decomposes to form low-molecular-weight compounds (LMWC) oxygenated molecular compounds (as those observed by Zhang et al., 2010) (5c), and RO$^\bullet$ radicals (von Sonntag and Schuchmann, 1997) (5a). ROO$^\bullet$ radicals can also react with MVK (or $HO_2^\bullet$) (4b) to form hydroperoxides ROOH. The latter can be photolyzed (5b) to yield HO$^\bullet$ and RO$^\bullet$ radicals. These alkoxy radicals undergo either rearrangement (6a) or decomposition (6b). The rearrangement of alkoxy radicals in aqueous medium is a well-known process (Schuchmann and von Sonntag, 1984), it produces (via pathway 6a) more stable radicals (R-OH)$^\bullet$ which undergo either O_2 reactivity (leading to some

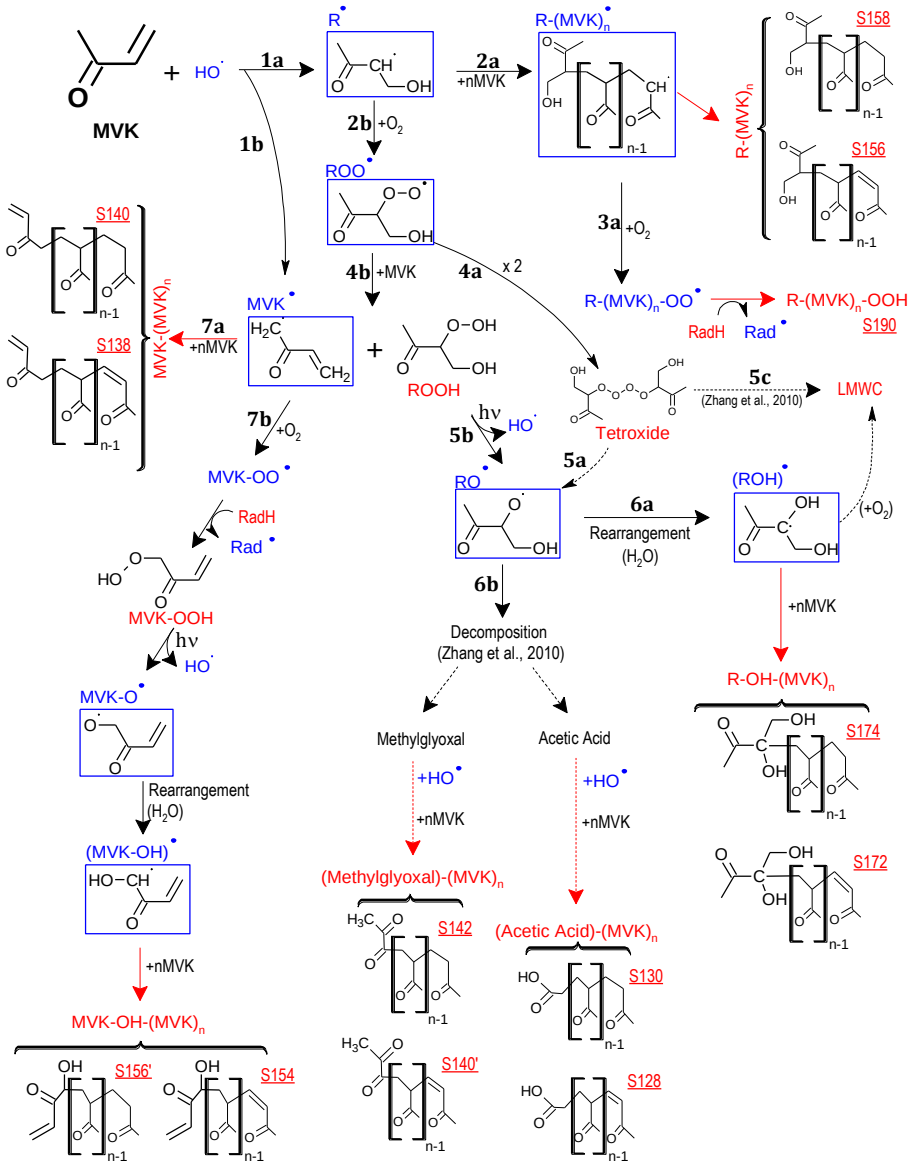

Fig. 10. Proposed scheme of the chemical mechanism of OH-oxidation of MVK in the aqueous phase with implementation of radical oligomerization pathways (for clarity, only external OH-addition on MVK is developed). RadH=MVK, $HO_2^\bullet$ or molecular reaction products (in red). Radicals (in blue). LMWC: low-molecular-weight compounds.

of the oxygenated molecular compounds observed by Zhang et al., 2010) or oligomerization with MVK via the disproportionation mechanism (Fig. 6) and form R-OH-(MVK)$_n$ (series S172, S174). The decomposition (pathway 6b, detailed in Zhang et al., 2010) produces smaller oxygenated compounds, such as methylglyoxal and acetic acid. The latter products react further with HO$^\bullet$ radicals to form radicals (as described by Tan et al., 2012) which undergo either O_2 reactivity or oligomerization with MVK via the disproportionation mechanism (Fig. 6) and form series S140′ and S142, and series S128 and S130, respectively.

3.4.2 Pathway 1b

H-abstraction leads to an unsaturated radical, MVK$^\bullet$, which can also be formed via pathway (4b), as mentioned above. MVK$^\bullet$ radicals undergo either oligomerization with MVK via the disproportionation mechanism (Fig. 6) and terminate (7a) into (MVK)-(MVK)$_n$ (series S138 and S140) or O_2 addition (7b) and further react to produce MVK-OH-(MVK)$_n$ (series S154 and S156′).

In this mechanism, the formed low-molecular-weight compounds (LMWC, such as formaldehyde, methylglyoxal, glyoxal, oxalic, formic, pyruvic, malonic and acetic acids, observed by Zhang et al. (2010) during the OH-oxidation of

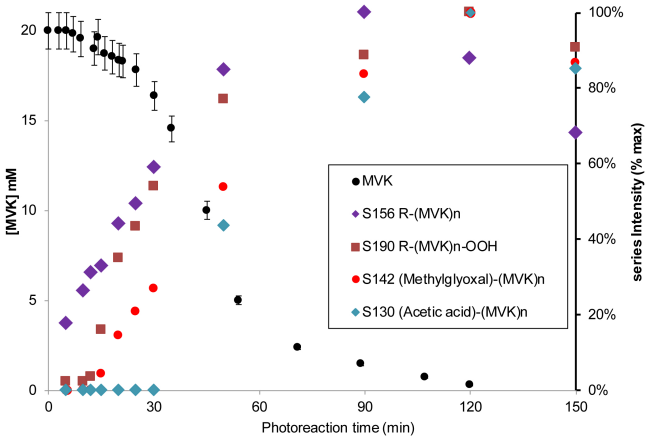

Fig. 11. MVK kinetics and time profile of main oligomers series (obtained using UPLC-ESI-MS, for the retention time range 0–7 min, in both modes) at 5 °C. The series intensity is the sum of the peaks intensity. Each series intensity is expressed as a percentage of its maximum.

MVK under similar conditions) can also further react with $HO^{\bullet}$ and produce other $iR^{\bullet}$ radicals, which can oligomerize. However, the corresponding oligomers were observed here only for acetic acid and methylglyoxal, which were among the major low-molecular-weight products observed by Zhang et al. (2010). A confirmation of these observations was brought by two extra experiments (A′ and A″) where 2 mM of methylglyoxal and acetic acid (Sigma Aldrich), respectively, were injected in the vessel at the same time as MVK injection. The results showed a significant increase (by 42 % and 77 %, respectively) of the corresponding oligomer series (S140′ and S142 and series S128 and S130, respectively), compared to experiment A. Furthermore, experiment C (performed at 5 °C) allowed us to clearly observe the kinetics of oligomer formation (Fig. 11). The series R-$(MVK)_n$ (S156) were directly formed, immediately followed by the series R-$(MVK)_n$-OOH (S190) (which require O_2 addition), and the series (Methylglyoxal)-$(MVK)_n$ (S142) and (Acetic acid)-$(MVK)_n$ (S130) were formed later, in very good agreement with the proposed mechanism (in Fig. 10).

The role of molecular O_2 was evidenced by the intensities of the identified series (Table 2). Comparing experiments A and D (i.e., from supersaturated to low initial O_2 conditions, respectively), after 50 min of reaction, a systematic increase of the intensities of all series not requiring O_2 addition were observed, as well as a systematic decrease of those requiring O_2 addition. This observation is also in very good agreement with the proposed mechanism (Fig. 10) described above, and it shows the prevailing role of oxygen on the processes.

4 Atmospheric implications

The proposed mechanism allowed for explaining the particular role of dissolved O_2 under our experimental conditions. Each $iR^{\bullet}$ radical underwent competition kinetics between O_2 addition (Reaction R1) and oligomerization (Reaction R2):

$$iR^{\bullet} + O_2 \rightarrow \text{LMWC} \quad k_{R1} \tag{R1}$$

$$iR^{\bullet} + n(\text{MVK}) \rightarrow \text{oligomers} \quad k_{R2} \tag{R2}$$

Supersaturated (by a factor of 155 %) initial O_2 concentrations inhibited radical oligomerization by fast addition on $iR^{\bullet}$ resulting in the formation of LMWC (such as acetic acid and methylglyoxal), which were further OH-oxidized and formed other $iR^{\bullet}$ radicals. The fast O_2 addition reactions resulted in a fast decrease of O_2 concentrations in the vessel, faster than O_2 renewal from the gas phase and from the reactivity of H_2O_2, and even faster than MVK consumption. At initial MVK concentrations higher than 0.2 mM, the decrease of O_2 concentrations resulted in the dominance of Reaction (R2) after several minutes, and oligomerization started, even when O_2 concentrations were still higher than Henry's law equilibrium with atmospheric O_2. The paradoxical role of O_2 resides in the fact that while it intensely inhibits oligomerization, it produces more $iR^{\bullet}$ radicals, which contribute to O_2 consumption, and thus lead to oligomerization. These processes, together with the large ranges of initial concentrations investigated (60–656 µM of dissolved O_2 and 0.2–20 mM of MVK concentrations) show the fundamental role that O_2 likely plays in atmospheric waters. In order to scale the relative importance of Reactions (R1) and (R2) from the laboratory to the atmospheric conditions, one has to compare the rates of Reactions (R1) and (R2):

$$v_{R1} = k_{R1} \times [iR^{\bullet}] \times [O_2]$$

$$v_{R2} = k_{R2} \times [iR^{\bullet}] \times [\text{MVK}]$$

The dominance of oligomerization over O_2 addition is determined by $\frac{v_{R2}}{v_{R1}} = \frac{k_{R2}}{k_{R1}} \times \frac{[\text{MVK}]}{[O_2]}$ $\frac{v_{R2}}{v_{R1}} = \frac{k_{R2}}{k_{R1}} \times \frac{[\text{MVK}]}{[O_2]}$. Assuming that the ratio $\frac{k_{R2}}{k_{R1}}$ does not vary from the laboratory conditions to the atmospheric ones, one can simply predict the oligomerization to occur from the $[\text{MVK}]/[O_2]$ ratio. In our experiments, the detailed study of the time profiles of O_2 and MVK together with the kinetics of oligomer formation allowed us to determine that radical oligomerization dominates over O_2 addition for $[\text{MVK}]/[O_2]$ ratios (in M M^{-1}) equal or higher than 32 (at 5 °C) and 54 (at 25 °C). In atmospheric waters, assuming that dissolved O_2 concentrations are saturated (i.e., at Henry's law equilibrium) everywhere from 0 to 5 km in altitude, and from −20 to +25 °C, gives a range of 190–391 µM for $[O_2]$. Furthermore, taking the concentrations of unsaturated organic compounds ([UNS]) in atmospheric waters as stated in the introduction, one obtains $[\text{UNS}]/[O_2]$ ratios as indicated in Fig. 12 (Ervens et al., 2012). In this figure, radical oligomerization occurs when $[\text{UNS}]/[O_2]$ ratios

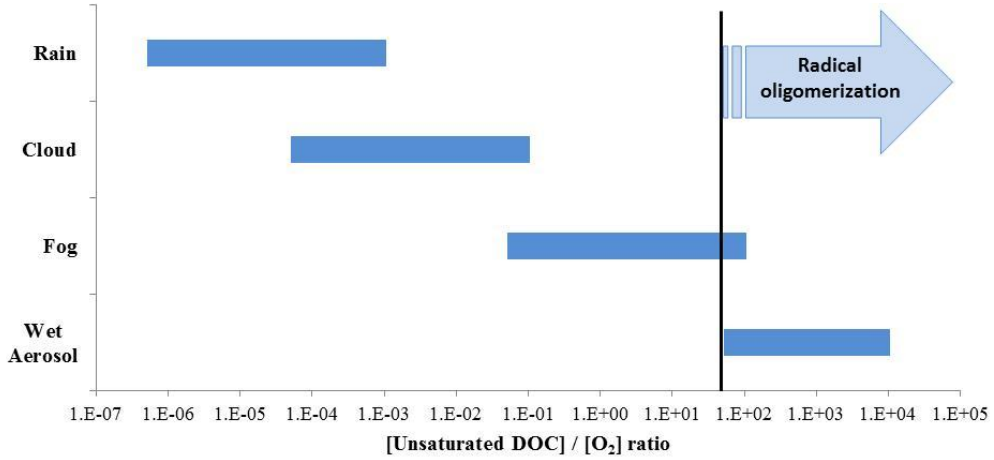

Fig. 12. Estimated ranges of the ratios of unsaturated dissolved organic carbon concentration to oxygen concentration (in $M\,M^{-1}$) in atmospheric waters. The straight lines delimit the values for which radical oligomerization dominates over O_2 addition, as determined by the present work (see text).

Table 3. Comparison of MVK atmospheric lifetimes between its gas phase reactivity only and its multiphase reactivity, taking into account its air/water partitioning at Henry's law equilibrium, its gas and aqueous phase reactivity: oligomerization is considered only in fogs and aerosol media, with k_{oligo} values derived from our experimental results.

	Gas	Multiphase in cloud		Multiphase in fog		Multiphase in aerosol
OH_{gas} concentration (molec cm^{-3})	10^6	10^6		10^6		10^6
OH_{aq} concentration (M)	–	10^{-13}		10^{-12}		10^{-11}
O_3 concentration (ppbV)	50	50		50		50
Radical oligomerization reactions	No	No		Yes[a]		Yes[a]
Henry's law constant (M atm^{-1})	–	41[b]		41[b]		7100[c]
LWC (g m^{-3})	–	5	1	0.4	0.1	2.5×10^{-5}
Atmospheric lifetimes (h) at 298 K	12	10.4	11.6	10.4	11.5	11.8
% impact of aqueous phase reactivity	–	−13 %	−3 %	−13 %	−4 %	−2 %

[a] $k_{oligo} = 8 \times 10^{-4}\,s^{-1}$; [b] Iraci et al. (1999); [c] Nozière et al. (2006).

are equal or higher than 32 or 54. It is thus concluded that radical oligomerization will always occur in wet aerosols, and in sometimes in fogs: in the most polluted fogs, where [UNS] > 6 mM. This result, added to the fact that the lifetime of wet aerosols in the atmosphere are several days, shows the extreme relevance of radical oligomerization of unsaturated organic compounds in the atmosphere.

Another point of view for atmospheric implications is the fate of MVK. In general, aqueous phase OH-oxidation is known to drastically reduce WSOCs atmospheric lifetimes, compared to their gas phase reactivity (Monod et al., 2005). As it was shown in the present study, once in the aqueous phase, MVK can undergo OH-oxidation. In fogs and wet aerosols, it can additionally undergo oligomerization with a first order kinetic rate constant of $k_{oligo} = 7.6\ (\pm 0.3) \times 10^{-4}\,s^{-1}$, (which is not temperature dependent between 5 and 25 °C) as derived in the present work from the MVK decay during oligomerization, under all conditions (Figs. 5 and 9). Although MVK is weakly water soluble, its (aerosol) aqueous phase reactivity may impact its overall atmospheric lifetime. In Table 3, MVK atmospheric lifetimes are compared between its gas phase reactivity only (taking into account both OH-oxidation and ozonolysis) and its multiphase reactivity. The latter takes into account MVK air/water partitioning at Henry's law equilibrium, and its aqueous phase reactivity: oligomerization is considered only in fogs and aerosol media. Table 3 shows that aqueous phase reactivity impacts the overall atmospheric lifetime of MVK by 2 to 13 %. Compared to these numbers, the rate of heterogeneous ozonolysis of MVK on SiO_2 or α-Al_2O_3 particles under various relative humidity ($\gamma = 10^{-10}$ to 10^{-9}, Shen et al., 2013) calculated for a number of 100 nm particles of 5000 particles cm^{-3}, would deplete its atmospheric lifetime by less than 0.00006 %. Thus, aqueous phase photooxidation seems more efficient, but this needs to be confirmed by more studies of both bulk and heterogeneous reactivity of olefin compounds.

The results obtained in Fig. 12 and Table 3 show the atmospheric relevance of (aerosol) aqueous phase reactivity of unsaturated water soluble organic compounds (even for low soluble ones like MVK), and their ability to activate radical oligomerization chemistry, which is extremely fast and is able to form macromolecules as high as 1800 Da in polluted fogs and wet aerosols. For an unsaturated compound 10 times more soluble than MVK, it is anticipated that its overall atmospheric lifetime would be depleted by 13 to 79 %, thus showing the need for further studies of oligomer formation from other relevant unsaturated compounds. In particular, the influence of other unsaturated compounds such as methacrolein on the chemistry detailed here is currently under study (G. Salque et al., personal communication, 2013). Furthermore, relevant mixtures of unsaturated compounds should be studied to investigate cross-polymerization reactions that are likely in the atmosphere. Finally, further studies are also needed to investigate the oligomer yields, their oxidizing states, and their aging (F. Siekmann et al., personal communication, 2013).

Supplementary material related to this article is available online at: http://www.atmos-chem-phys.net/13/6473/2013/acp-13-6473-2013-supplement.pdf.

Acknowledgements. We thank the National Research Agency ANR (project Cumulus), AXA insurances and CNRS-INSU for funding this research. We also thank Barbara Ervens (CIRES, University of Colorado, Boulder and Chemical Sciences Division, National Oceanic and Atmospheric Administration (NOAA), Boulder, CO, USA) and Gaëlle Gosset (Aix Marseille Université, CNRS, ICR UMR7273, 13397, Marseille, France) for valuable scientific discussions on this topic.

Edited by: M. Ammann

References

Alarifi, A. and Aouak, T.: Homopolymerization of benzylmethacrylate and methylvinylketone using Ni(acac)$_2$-methylaluminoxane catalyst system, Arabian Journal of Chemistry 2, 87–93, 2009.

Baduel, C., Voisin, D., and Jaffrezo, J.-L.: Seasonal variations of concentrations and optical properties of water soluble HULIS collected in urban environments, Atmos. Chem. Phys., 10, 4085–4095, doi:10.5194/acp-10-4085-2010, 2010.

Bateman, A. P., Walser, M. L., Desyaterik, Y., Laskin, J., Laskin, A., and Nizkorodov, S. A.: The Effect of Solvent on the Analysis of Secondary Organic Aerosol Using Electrospray Ionization Mass Spectrometry, Environ. Sci. Technol., 42, 7341–7346, doi:10.1021/es801226w, 2008.

Benson, B. B. and Krause, D.: The concentration and isotopic fractionation of oxygen dissolved in freshwater and seawater in equilibrium with the atmosphere, American Society of Limnology and Oceanography Inc., Department of Physics, Amherst College, Amherst, Massachusetts, USA, 1984.

Carlton, A. G., Wiedinmyer, C., and Kroll, J. H.: A review of Secondary Organic Aerosol (SOA) formation from isoprene, Atmos. Chem. Phys., 9, 4987–5005, doi:10.5194/acp-9-4987-2009, 2009.

Claeys, M., Wang, W., Ion, A. C., Kourtchev, I., Gelencsér, A., and Maenhautc, W.: Formation of secondary organic aerosols from isoprene and its gas-phase oxidation products through reaction with hydrogen peroxide, Atmos. Environ., 38, 4093–4098, 2004.

Claeys, M., Kourtchev, I., Pashynska, V., Vas, G., Vermeylen, R., Wang, W., Cafmeyer, J., Chi, X., Artaxo, P., Andreae, M. O., and Maenhaut, W.: Polar organic marker compounds in atmospheric aerosols during the LBA-SMOCC 2002 biomass burning experiment in Rondônia, Brazil: sources and source processes, time series, diel variations and size distributions, Atmos. Chem. Phys., 10, 9319–9331, doi:10.5194/acp-10-9319-2010, 2010.

Danger, G., Orthaus-Daunay, F. R., de Marcellus, P., Modica,P., Vuitton, V., Duvernay, F., Flandinet, L., Le Sergeant d'Hendecourt, L., Thissen, R., and Chiavassa, T.: Characterization of laboratory analogs of interstellar/cometary organic residues using very high resolution mass spectrometry, Geochim. Cosmochim. Ac., accepted, 2013.

Decesari, S., Facchini, M. C., Fuzzi, S., McFiggans, G. B., Coe, H., and Bower, K. N.: The water-soluble organic component of size-segregated aerosol, cloud water and wet depositions from Jeju Island during ACE-Asia, Atmos. Environ., 39, 211–222, 2005.

Decker, C. and Jenkins A. D.: Kinetic approach of O_2 inhibition in ultraviolet- and laser-induced polymerizations, Macromolecules, 18, 1241, doi:10.1021/ma00148a034, 1985.

El Haddad, I., Yao Liu, Nieto-Gligorovski, L., Michaud, V., Temime-Roussel, B., Quivet, E., Marchand, N., Sellegri, K., and Monod, A.: In-cloud processes of methacrolein under simulated conditions – Part 2: Formation of secondary organic aerosol, Atmos. Chem. Phys., 9, 5107–5117, doi:10.5194/acp-9-5107-2009, 2009.

Ervens, B. and Volkamer, R.: Glyoxal processing by aerosol multiphase chemistry: towards a kinetic modeling framework of secondary organic aerosol formation in aqueous particles, Atmos. Chem. Phys., 10, 8219–8244, doi:10.5194/acp-10-8219-2010, 2010.

Ervens, B., Turpin, B. J., and Weber, R. J.: Secondary organic aerosol formation in cloud droplets and aqueous particles (aqSOA): a review of laboratory, field and model studies, Atmos. Chem. Phys., 11, 11069–11102, doi:10.5194/acp-11-11069-2011, 2011.

Ervens, B., Wang, Y., Eagar, J., Leaitch, W. R., Macdonald, A. M., Valsaraj, K. T., and Herckes, P.: Dissolved organic carbon (DOC) and select aldehydes in cloud and fog water: the role of the aqueous phase in impacting trace gas budgets, Atmos. Chem. Phys. Discuss., 12, 33083–33125, doi:10.5194/acpd-12-33083-2012, 2012.

Fu, P., Kawamura, K., Usukura, K., and Miura, K.: Dicarboxylic acids, ketocarboxylic acids and glyoxal in the marine aerosols collected during a round-the-world cruise, Mar. Chem., 148, 22–32, 2013.

Gibian, M. J. and Corley, R. C.: Organic radical-radical reactions. Disproportionation vs. combination, Chem. Rev., 73, 441–464, doi:10.1021/cr60285a002, 1973.

Guzmàn, M. I., Colussi, A. J., and Hoffmann, M. R.: Photoinduced oligomerization of aqueous pyruvic acid, J. Phys. Chem. A, 110, 3619–3626, doi:10.1021/jp056097z, 2006.

Hallquist, M., Wenger, J. C., Baltensperger, U., Rudich, Y., Simpson, D., Claeys, M., Dommen, J., Donahue, N. M., George, C., Goldstein, A. H., Hamilton, J. F., Herrmann, H., Hoffmann, T., Iinuma, Y., Jang, M., Jenkin, M. E., Jimenez, J. L., Kiendler-Scharr, A., Maenhaut, W., McFiggans, G., Mentel, Th. F., Monod, A., Prévôt, A. S. H., Seinfeld, J. H., Surratt, J. D., Szmigielski, R., and Wildt, J.: The formation, properties and impact of secondary organic aerosol: current and emerging issues, Atmos. Chem. Phys., 9, 5155–5236, doi:10.5194/acp-9-5155-2009, 2009.

Herckes, P., Hannigan, M. P., Trenary, L., Lee, T., and Collett Jr., J. L.: Organic compounds in radiation fogs in Davis (California), Atmos. Res., 64, 99–108, 2002.

Herckes, P., Leenheer J. A., and Collett Jr., J. L.: Comprehensive Characterization of Atmospheric Organic Matter in Fresno, California Fog Water, Environ. Sci. Technol., 41, 393–399, 2007.

Herrmann, H., Hoffmann, D., Schaefer, T., Bräuer, P., and Tilgner, A.: Tropospheric aqueous phase free radical chemistry: radical sources, spectra, reaction kinetics and prediction tools, Chem. Phys. Chem., 11, 3796–3822, 2010.

Hobby, K.: Micromass MS Technologies, Floats Road, Manchester, M23 9LZ, UK, A novel method of isotope prediction applied to elemental composition analysis, Waters Corporation, 2005.

Huang, D., Zhang, X., Chen, Z. M., Zhao, Y., and Shen, X. L.: The kinetics and mechanism of an aqueous phase isoprene reaction with hydroxyl radical, Atmos. Chem. Phys., 11, 7399–7415, doi:10.5194/acp-11-7399-2011, 2011.

Hughey, C. A., Hendrickson, C. L., Rodgers, R. P., and Marshall, A. G.: Kendrick Mass Defect Spectrum: A Compact Visual Analysis for Ultrahigh-Resolution Broadband Mass Spectra, Anal. Chem., 73, 4676–4681, 2001.

Iraci, L. T., Baker, B. M., Tyndall, G. S., and Orlando, J. J.: Measurements of the Henry's law coefficients of 2-methyl-3-buten-2-ol, methacrolein, and methyl vinyl ketone, J. Atmos. Chem., 33, 321–330, 1999.

Kawamura, K. and Ikushima, K.: Seasonal Changes in the Distribution of Dicarboxylic Acids in the Urban Atmosphere, Environ. Sci. Technol., 27, 2227–2235, 1993.

Kawamura, K., Kasukabe, H., and Barrie, L. A.: Source and reaction pathways of dicarboxylic acids, ketoacids and dicarbonyls in arctic aerosols: one year of observations, Atmos. Environ., 30, 1709–1722, 1996.

Li, Y. and Schellhorn, H. E.: Rapid kinetic microassay for catalase activity, Journal of Biomolecular Techniques, 18, 185–187, 2007.

Liao, H. and Seinfeld, J. H.: Global impacts of gas-phase chemistry-aerosol interactions on direct radiative forcing by anthropogenic aerosols and ozone, J. Geophys. Res.-Atmos., 110, D18208, doi:10.1029/2005JD005907, 2005.

Lim, Y. B., Tan, Y., Perri, M. J., Seitzinger, S. P., and Turpin, B. J.: Aqueous chemistry and its role in secondary organic aerosol (SOA) formation, Atmos. Chem. Phys., 10, 10521–10539, doi:10.5194/acp-10-10521-2010, 2010.

Liu, Y.: Etudes des impacts de la réactivité en phase aqueuse atmosphérique sur la formation et le vieillissement des Aérosols Organiques Secondaires sous conditions simulées, Ph.D. thesis, Laboratoire de Chimie de l'Environnement, Aix-Marseille University, France, 2011.

Liu, Y., Siekmann, F., Renard, P., El Zein, A., Salque, G., El Haddad, I., Temime-Roussel, B., Voisin, D., Thissen, R., and Monod, A.: Oligomer and SOA formation through aqueous phase photooxidation of methacrolein and methyl vinyl ketone, Atmos. Environ., 49, 123–129, doi:10.1016/j.atmosenv.2011.12.012, 2012.

Makarov, A., Denisov, E., Lange, O., and Horning, S.: Dynamic Range of Mass Accuracy in LTQ Orbitrap Hybrid Mass Spectrometer, J. Am. Soc. Mass Spectr., 17, 977–982, doi:10.1016/j.jasms.2006.03.006, 2006.

Monod, A., Poulain, L., Grubert, S., Voisin, D., and Wortham, H.: Kinetics of OH-initiated oxidation of oxygenated organic compounds in the aqueous phase: new rate constants, structure-activity relationships and atmospheric implications, Atmos. Environ., 39, 7667–7688, 2005.

Nozière, B., Voisin, D., Longfellow, C. A., Friedli, H., Henry, B. E., and Hanson, D. R.: The Uptake of Methyl Vinyl Ketone, Methacrolein, and 2-Methyl-3-butene-2-ol onto Sulfuric Acid Solutions, J. Phys. Chem. A, 110, 2387–2395, 2006.

Odian, G.: Principles of polymerization, published by John Wiley & Sons, Inc., Hoboken, New Jersey, 200–205, 2004.

Orthous-Daunay, F. R.: Empreinte moléculaire des processus post-accrétionnels dans la matière organique des chondrites carbonées, Ph.D. thesis, Institut de Planetelogie et d'Astrophysique, Université Joseph Fourier in Grenoble, France, 2011.

Ortiz-Montalvo, D. L., Lim, Y. B., Perri, M. J., Seitzinger, S. P., and Turpin, B. J.: Volatility and Yield of Glycolaldehyde SOA Formed through Aqueous Photochemistry and Droplet Evaporation, Aerosol Sci. Tech., 46, 1002–1014, 2012.

Pearce, E. M., Wright, C. E., and Bordoloi, B. K.: Laboratory Experiments in Polymer Synthesis and Characterization, Educational Modules for Materials Science and Engineering Project, Elsevier, USA, 1–22, 1982.

Schuchmann, H.-P. and von Sonntag, C.: Methylperoxyl radicals: a study of the γ-radiolysis of methane in oxygenated aqueous solutions, Z. Naturforsch. B, 39, 217–221, 1984.

Sempéré, R. and Kawamura, K.: Comparative distributions of dicarboxylic acids and related polar compounds in snow, rain and aerosols from urban atmosphere, Atmos. Environ., 28, 449–459, 1994.

Shen, X., Zhao, Y., Chen, Z., and Huang, D.: Heterogeneous reactions of volatile organic compounds in the atmosphere, Atmos. Environ., 68, 297–314, 2013.

Tan, Y., Carlton, A. G., Seitzinger, S. P., and Turpin, B. J.: SOA from methylglyoxal in clouds and wet aerosols: Measurement and prediction of key products, Atmos. Environ., 44, 5218–5226, 2010.

Tan, Y., Lim, Y. B., Altieri, K. E., Seitzinger, S. P., and Turpin, B. J.: Mechanisms leading to oligomers and SOA through aqueous photooxidation: insights from OH radical oxidation of acetic acid and methylglyoxal, Atmos. Chem. Phys., 12, 801–813, doi:10.5194/acp-12-801-2012, 2012.

van Pinxteren, D., Plewka, A., Hofmann, D., Müller, K., Kramberger, H., Svrcina, B., Bächmann, K., Jaeschke, W., Mertes, S., Collett Jr., J. L., and Herrmann, H.: Schmücke hill cap cloud and valley stations aerosol characterisation during FEBUKO (II): organic compounds, Atmos. Environ., 39, 4305–4320, 2005.

Volkamer, R., SanMartini, F., Molina, L. T., Salcedo, D., Jimenez, J., and Molina, M. J.: A missing sink for gas-phase glyoxal in Mexiko City: formation of secondary organic aerosol, Geophys. Res. Lett., 34, L19807, doi:10.1029/2007GL030752, 2007.

Volkamer, R., Ziemann, P. J., and Molina, M. J.: Secondary Organic Aerosol Formation from Acetylene (C_2H_2): seed effect on SOA yields due to organic photochemistry in the aerosol aqueous phase, Atmos. Chem. Phys., 9, 1907–1928, doi:10.5194/acp-9-1907-2009, 2009.

von Sonntag, C. and Schuchmann, H.-P.: Peroxyl radicals in aqueous solution, in: Peroxyl Radicals, edited by: Alfassi, Z. B., Wiley, Chichester, 173–234, 1997.

Yadav, L. D. S.: Organic Spectroscopy, Kluwer Academic, Secaucus, NJ, USA, 7–51, 2012.

Yao Liu, El Haddad, I., Scarfogliero, M., Nieto-Gligorovski, L., Temime-Roussel, B., Quivet, E., Marchand, N., Picquet-Varrault, B., and Monod, A.: In-cloud processes of methacrolein under simulated conditions – Part 1: Aqueous phase photooxidation, Atmos. Chem. Phys., 9, 5093–5105, doi:10.5194/acp-9-5093-2009, 2009.

Zhang, X., Chen, Z. M., and Zhao, Y.: Laboratory simulation for the aqueous OH-oxidation of methyl vinyl ketone and methacrolein: significance to the in-cloud SOA production, Atmos. Chem. Phys., 10, 9551–9561, doi:10.5194/acp-10-9551-2010, 2010.

Ziaee, F., Bouhendi, H., and Ziaie, F.: NMR Study of Polyacrylamide Tacticity Synthesized by Precipitated Polymerization Method, I. Poly. J., 18, 947–956, 2009.